RESEARCH ARTICLE

•Arch Hyg Sci 2017;6(1): 17-25
•Journal Homepage: http://jhygiene.muq.ac.ir

Removal of Cr(VI) Ions from Aqueous Solutions Using Nickel Ferrite Nanoparticles: Kinetic and Equilibrium Study

RaziyehZandipak[a]*

[a]Young Researchers and Elite Club, Hamedan Branch, Islamic Azad University, Hamedan, Iran.

***Correspondence** should be addressed to Mis. Raziyeh Zandipak, **Email:**raziyeh.zandi@yahoo.com

A-R-T-I-C-L-EI-N-F-O

Article Notes:
Received: Aug.20, 2016
Received in revised form: Nov.10, 2016
Accepted: Nov. 20, 2016
Available Online: Jan 1, 2017

Keywords:
Nanoparticles
Adsorption
Isotherm
Chromium
Nickel Ferrite
Iran

A-B-S-T-R-A-C-T

Background & Aims of the Study: Heavy metals are the most important and main pollutants because of their accumulation and high toxicity even at very low dose and cause serious hazards to ecological system as well as human health. Thus, their removal has been challenged from drinking water and industrial waters with different technologies. The purpose of this work is to investigate the removal of Cr(VI) from aqueous solutions.

Materials & Methods: $NiFe_2O_4$ nanoparticles was prepared by the co-precipitation method and then applied for adsorption of Cr(VI) ions from water. Characterization of nanoparticles was carried out via TEM, EDX, XRD and BET analysis. Various physico-chemical parameters like the effect of contact time, pH and adsorbent dose were studied, using batch process to optimize conditions for maximum adsorption.

Results: The results demonstrated that the size of the $NiFe_2O_4$ nanoparticles was about 12 nm and had selectivity for Cr(VI) adsorption. Also, adsorption process was found to be fast with equilibrium time of 55 min. Optimum pH was found to be 3. Maximum adsorption capacity (q_m) as calculated from Langmuir isotherm was found to be 294.1 mg g^{-1}. Analysis of adsorption kinetics indicated better applicability of pseudo-second-order kinetic model.

Conclusions: The results of this study represented that the synthesized $NiFe_2O_4$ nanoparticles could be useful for the simultaneous removal of anionic ions from wastewaters.

Please cite this article as: Zandipak R. Removal of Cr(VI) Ions from Aqueous Solutions Using Nickel Ferrite Nanoparticles: Kinetic and Equilibrium Study. Arch HygSci 2017;6(1):17-25.

Background

Chromium (Cr) is a generally heavy metal contaminate because of its highly toxic and bio-accumulatively (1). It is carcinogenic, mutagenic and thus is a threat to human health. In natural environments, chromium can exist mostly in two stable oxidation states: Cr(III) and Cr(VI). Among these two, hexavalent chromium exerts the most damaging toxic effects on living organisms, being highly soluble and mobile in water(2). In aqueous solution Cr(VI) exists as chromate (CrO_4^{2-}), hydrogen chromate ($HCrO_4^-$), dichromate ($Cr_2O_7^{2-}$) and hydrogen dichromate ($Cr_2O_7^-$)(3,4). Cr(VI) used in various industries, including leather tanning, stainless steels production, preparation of pigments and dyes, glass and ceramics, battery, metal electroplating and wood preservation etc (5,6). Cr(VI) has been reported to have detrimental effects on lungs, livers, kidney and nervous system of mammals (7,8). The US Environmental Protection Agency has set the maximum total Cr content in drinking water as 0.1 mg L^{-1} (9). Thus, the removal of low concentration of Cr(VI) ions from wastewater is very significant (10). Various technologies have been used to remove Cr(VI) from water such as adsorption, chemical treatment, ion exchange, membrane

process and electrochemical precipitation (11). Adsorption has been most widely utilized owing to availability, ease of operation, economical method and effective in comparison with other customary methods (12,13).

$NiFe_2O_4$ nanoparticles with the general formula MFe_2O_4 (M=Fe, Co, Ni, Zn, Cu, Mn, etc.) are the most popular materials in removal of heavy metals from water because of their large surface area, low toxicity, easy preparation and the unique advantage of easy separation under external magnetic fields (14,15). This material is also ferrimagnetic as a result of parallel alignment of the spins of the Fe^{3+} ions at tetrahedral sites and both the Ni^{2+} and Fe^{3+} ions at octahedral sites. Moreover, the magnetic behavior of these nanoparticles depends mostly on their size (16,17).

Aims of the study:

This work has studied the efficiency of $NiFe_2O_4$ nanoparticles as an adsorbent for adsorption of Cr(VI) from an aqueous solution. The adsorption studies were carried out at different pH values, different adsorbent dose and contact time in a batch experiments. In addition, the kinetic and isotherm parameters of the adsorption were computed and the mechanism of Cr(VI) adsorption on $NiFe_2O_4$ nanoparticles was discussed.

Materials & Methods

The concentration of Cr(VI) ions was measured, using inductively coupled plasma optical emission spectrometry (ICP-OES) (JY138 ultrace, France). A pH meter (780, Metrohm, Herisau, Switzerland) equipped with a combined Ag/AgCl glass electrode was used for pH measurements. The structure of synthesized nanoparticles was determined by XRD (38066 Riva, d/G.Via M. Misone, 11/D (TN) Italy) at ambient temperature. The structure of the $NiFe_2O_4$ nanoparticles was characterized by a transmission electronic microscopy (TEM, Philips, CM10, 100 KV). Specific surface area and porosity were defined by N_2 adsorption–desorption porosimetry (77 K), using a porosimeter (Bel Japan, Inc.). The elemental analysis was measured by scanning electron microscope energy dispersive X-ray spectroscopy (SEM-EDX, XL 30 and Philips Netherland).

All chemicals were of analytical grade available from Merck (Merck, Darmstadt, Germany) and used without further purification. Cr(VI) stock solution was prepared by dissolving $K_2Cr_2O_7$ in double-distilled water. The solutions of different initial concentrations were prepared by diluting the stock solution in appropriate proportions.

Synthesis of $NiFe_2O_4$ nanoparticles

The $NiFe_2O_4$ samples were synthesized by the co-precipitation method. Thus, 0.2 M (20 mL) solution of iron nitrate [$(Fe(NO_3)_3.9H_2O)$] and 0.1 M (20 mL) solution of nickel nitrate [$(Ni(NO_3)_2.6H_2O)$] were prepared and vigorously mixed under stirring for 1 h at 80 ^oC. 0.2 g of polyethylene oxide (PEO) was added into the solution as a capping agent. Subsequently, 5 ml of hydrazine hydrate ($NH_2.NH_2.H_2O$) was added drop by drop into the solutions and brown color precipitates were formed. Finally, the precipitates were separated by centrifugation and dried in hot air oven for 4 h at 100 ^oC. The acquired substance was annealed for 10 h at 300 ^oC (18).

Point of zero charge pH

The point of zero charge pH (pHpzc) for the adsorbent was determined by introducing 0.01 g of $NiFe_2O_4$ nanoparticles into eight 100 mL Erlenmeyer flasks containing 0.1 M $NaNO_3$ solution. The pH values of the solutions were adjusted at a range of 2-9 using solutions of 0.01 mol L^{-1} HNO_3 and/or NaOH solutions. The solution mixtures were allowed to equilibrate in an isothermal shaker (25 °C) for 24 h. The final pH was measured after 24 h. The pHpzc is the point where the pH initial=pH final (19).

Batch adsorption experiments

Cr(VI) ions removal studies with 0.002–0.04 g of $NiFe_2O_4$ nanoparticles were carried out in 25 mL stoppered conical flask containing 15 ml of

Cr(VI) solution of concentration 20 mg L^{-1}. The pH of the solution was adjusted to 2–10, using 0.1 mol L^{-1} HCl and/or 0.1 mol L^{-1}NaOH solutions. The mixture was placed in a thermostatic shaker (180 rpm and 25 °C). Samples were withdrawn at different time intervals (0–70 min), metal loaded $NiFe_2O_4$ nanoparticles were separated with magnetic decantation and the residual concentration of Cr(VI) ions in the bulk (C_e) was measured by an ICP-OES analysis. The concentration of the Cr(VI) ions remained in the adsorbent phase (q_e, mg g^{-1}) was evaluated, using equation (1):

$$q_e = \frac{(C_0-C_e)V}{W} (1)$$

where C_0 and C_e (mg L^{-1}) are initial and equilibrium concentrations, respectively, V (L) is the volume of solution and W (g) is the mass of adsorbent (20).

The Cr(VI) ions removal efficiency was evaluated, using equation (2):

$$R\ (\%) = \frac{C_0-C_e}{C_0} \times 100 (2)$$

Results

The TEM micrograph and calculated histogram of the $NiFe_2O_4$ nanoparticles are shown in Figure 1. The X-ray diffraction pattern of $NiFe_2O_4$ nanoparticles is shown in Figure 2. Also, Figure 3 represents a typical SEM-EDX elemental analysis of $NiFe_2O_4$ nanoparticles.

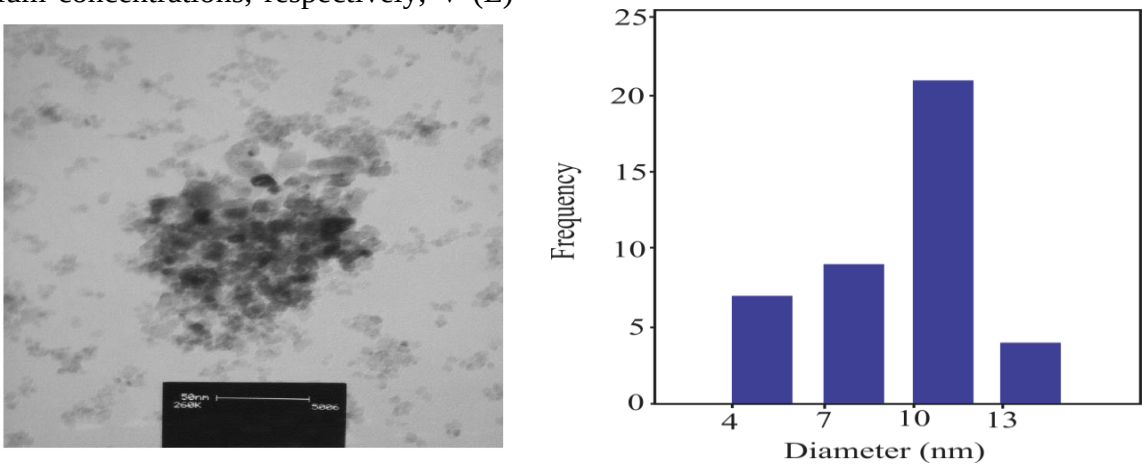

(a) (b)

Figure 1) (a) TEM micrograph and (b) calculated histogram of $NiFe_2O_4$ nanoparticles

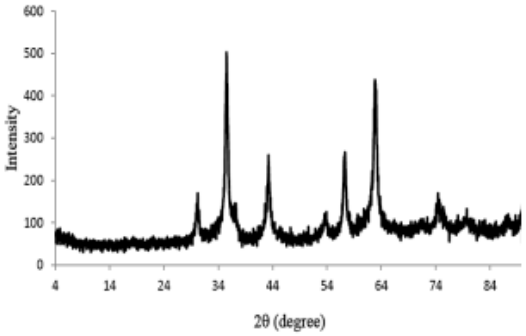

Figure 2) The X-ray diffraction pattern of $NiFe_2O_4$ nanoparticles.

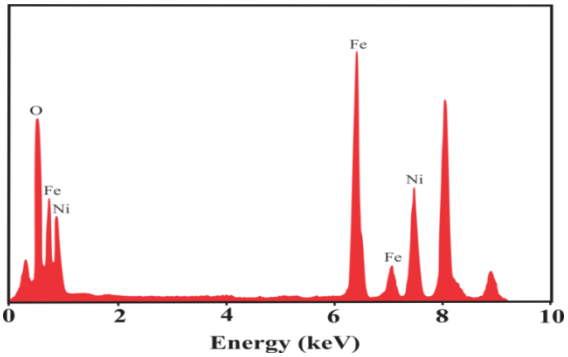

Figure 3) SEM-EDX spectrum of $NiFe_2O_4$ nanoparticles.

The pHpzc is an important characteristic that indicates the electrical neutrality of the surface of the adsorbent at a particular value of pH. The

point of zero charge (pHpzc) value determined for $NiFe_2O_4$ nanoparticles was 7.0 (Figure 4a). Effect of the pH on the adsorption of Cr(VI) ions with $NiFe_2O_4$ nanoparticles (Figure 4b) demonstrated that the adsorption percentage of Cr(VI) ions onto $NiFe_2O_4$ nanoparticles decreased with an increase in the pH from 3.0–10.0.

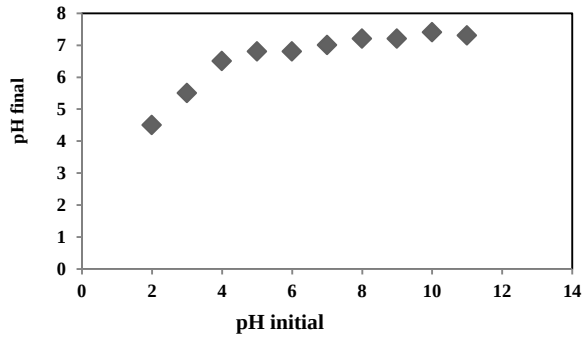

(a)

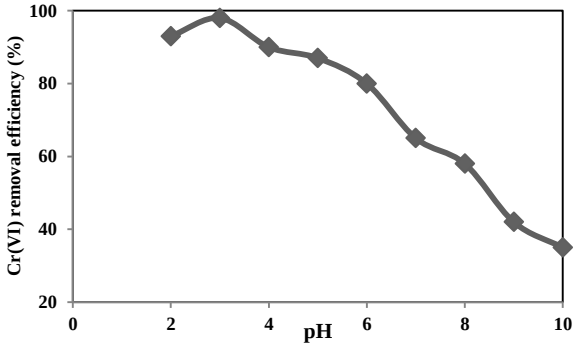

(b)

Figure 4) (a) The determination of the point of zero charge of the $NiFe_2O_4$ nanoparticles. (b) Effect of solution pH on the removal percentage of Cr(VI) by $NiFe_2O_4$ nanoparticles.

Adsorbent dose is a significant parameter that effect in adsorption studies because it determines the removal capacity of adsorbent for a given initial concentration of metal ion solution. In the present study, the adsorbent dose was varied from 0.002 to 0.04 g at fixed Cr(VI) concentration of 20 mg L^{-1}. The obtained results are shown in Figure 5 which reveals that the removal efficiency is maximum (98.5) at Cr(VI) dose of 0.01 g.

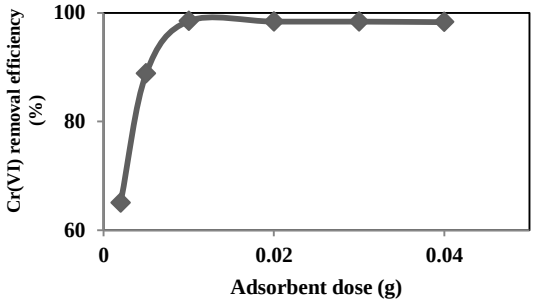

Figure 5) Effect of dose of NiFe2O4 nanoparticles on the removal percentage of Cr(VI) ions.

The effect of adsorption time was studied at initial concentrations of 20, 70 and 140 mg L^{-1}, respectively. Adsorption tests were carried out in a time interval between 0 and 70 min. As Figure 6 shows, equilibrium for Cr(VI) ions was reached within 55 min.

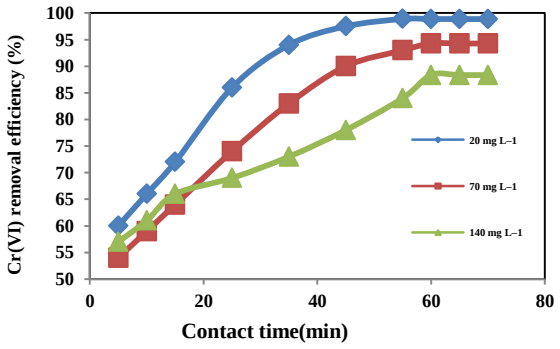

Figure 6) Effect of contact time on the removal percentage of Cr(VI) ions.

To analyze the adsorption kinetic rate constant of Cr(VI) ions onto $NiFe_2O_4$ nanoparticles, pseudo-first-order and pseudo-second-order models were applied to the experimental data. Different kinetic parameters of both models are listed in Table 1. Also, the linear fitting of kinetics models are shown in Figure 7.

Table 1) Pseudo-first order and pseudo-second order kinetic model parameters for the adsorption of Cr(VI) ions onto $NiFe_2O_4$ nanoparticles at 25°C.

		Pseudo-first-order kinetic model				Pseudo-second-order kinetic		
	C_0 (mg L^{-1})	$q_e$exp(mg g^{-1})	q_{e1}(mg g^{-1})	k_1 (min^{-1})	R^2	q_{e2} (mg g^{-1})	k_2 (g mg^{-1} min^{-1})	R^2
Cr(VI)	20	49.44	93.50	0.129	0.842	50.29	0.002	0.998
	70	165.0	352.8	0.114	0.839	169.67	0.005	0.998
	140	309.2	625.1	0.109	0.734	323.33	0.003	0.998

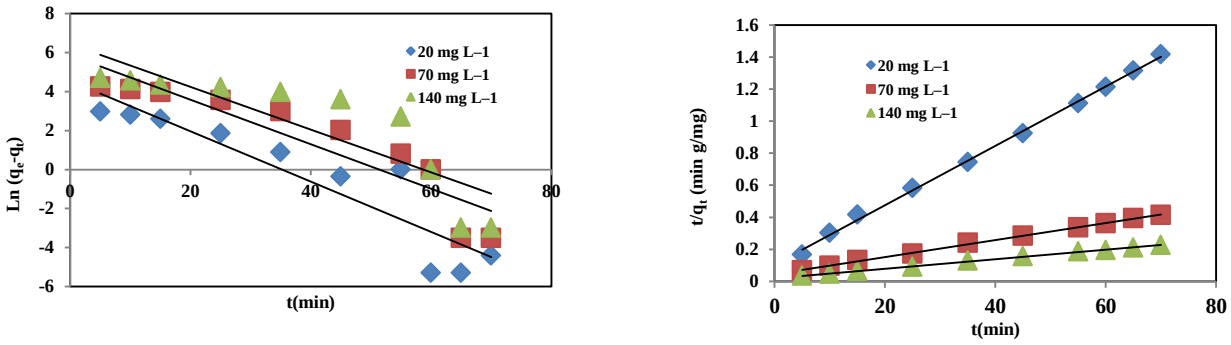

(a) **(b)**

Figure 7) (a) Pseudo-first-order kinetic plot, and (b) pseudo-second-order kinetic plot for the adsorption of Cr(VI) ions onto $NiFe_2O_4$ nanoparticles at 25°C.

To evaluate the equilibrium adsorption data in this work, two usual isotherm models, like the Langmuir and Freundlich models are used to explain the equilibrium data. The adsorption isotherms for Cr(VI) ions onto $NiFe_2O_4$nanoparticles at 25 °C are shown in Figure 8. The isotherm constants for the adsorption of Cr(VI) ions on $NiFe_2O_4$ nanoparticles are listed in Table 2

Table 2) Isotherm parameters of adsorption of Cr(VI) ions onto $NiFe_2O_4$ nanoparticles at 25 °C.

Langmuir				Freundlich		
b (L mg^{-1})	q_m (mg g^{-1})	R_L	R^2	K_f($mg^{1-(1/n)}$ $L^{1/n}$ g^{-1})	n	R^2
0.078	294.1	0.390	0.996	58.90	3.342	0.980

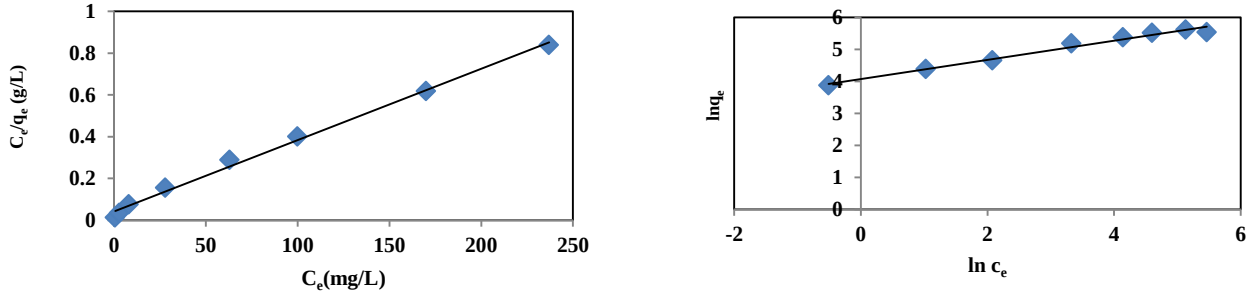

(a) **(b)**

Figure 8) (a) Langmuir and (b) Freundlich isotherms for adsorption of Cr(VI) ions onto $NiFe_2O_4$ nanoparticles at 25 °C.

Discussion

The TEM micrograph and calculated histogram of the $NiFe_2O_4$ nanoparticles revealed that the size of the synthesized $NiFe_2O_4$ nanoparticles was about 12 nm (Figure 1). Figure 2 displays the X-ray diffraction (XRD) patterns of $NiFe_2O_4$ nanoparticles, where all the diffraction peaks of $NiFe_2O_4$ nanoparticles are assigned to spinel type $NiFe_2O_4$ (JCPDS 54-0964). The peaks at the 2Θ values of 30.1, 35.3, 43.0, 53.7, 56.5, and 62.4° can be indexed to (111), (220), (311), (400), (422), (511) and (440) crystal planes of spinel $NiFe_2O_4$, respectively. Figure 3 shows a typical SEM-EDX elemental analysis of $NiFe_2O_4$ nanoparticles. The results illustrate that only Ni, Fe, and O appear in $NiFe_2O_4$ nanoparticles sample.

Specific surface areas are usually reported as BET surface areas obtained by applying the theory of Brunauer, Emmett, and Teller (BET) to nitrogen adsorption/desorption isotherms measured at 77 K. This is a standard procedure for the determination of the specific surface area of sample. The specific surface area of the sample is determined by physical adsorption of a gas on the surface of the solid and by measuring the amount of adsorbed gas corresponding to a monomolecular layer on the surface. The data are treated according to the BET theory (21,22). The results of the BET method demonstrated that the average specific surface area of $NiFe_2O_4$ nanoparticles was 63.7 $m^2\ g^{-1}$. It can be concluded from these values that the synthesized nanoparticles have relatively large specific surface areas and may be better for adsorption.

As shown in Figure 4b, the removal percentage decreased sharply with the increase of pH from 3.0 to 10.0. The adsorption was higher in lower acidic solutions with a maximum adsorption efficiency of 98.0 % at pH 3.0. This could be explained by the pHzpc of the $NiFe_2O_4$ nanoparticles, which is illustrated in Figure 4a. The point of zero charge (pHpzc) value determined for $NiFe_2O_4$ nanoparticles was 7.0. When the solution pH was lower than 7.0, the $NiFe_2O_4$ nanoparticles was positively charged and so anion Cr(VI) existing as $HCrO_4^-$and CrO_4^{2-} adsorption occurred. When the solution pH was higher than 7.0, the $NiFe_2O_4$ nanoparticles was negatively charged. Thus electrostatic repulsion between negatively charged Cr(VI) species and the negatively charged $NiFe_2O_4$ nanoparticles would increase. This would result in a release of the adsorbed $HCrO_4^-$ and CrO_4^{2-}. The removal percentage of Cr(VI) decreased with the increase of pH. This was also due to the higher concentration of OH^- ions existing in the working solutions. The varying of the adsorption capacity may be ascribed to various chromium species. In fact, the Cr(VI) in solution exists in the form of oxyanions such as $HCrO_4$–, CrO_4^{2-} and $Cr_2O_7^{2-}$. The dominant form of Cr(VI) is $HCrO_4^-$ at lower pH (1.0–5.0). As the pH rises, the dominant species of Cr(VI) are CrO_4^{2-}, $Cr_2O_7^{2-}$. A similar behavior has been reported for Cr(VI) removal on Magnetite nanospheres (23).

Figure 5 shows the effect of adsorbent dosage on the adsorption efficiency of Cr(VI) from water. It is observed that the removal percentage increases from 65% to 98.5% with an increase in adsorbent dosage from 0.002 to 0.01 g. This is because of an increase in the surface area and availability of more active sites for adsorption. Afterwards, the removal efficiency remains unchanged with increase in adsorbent dosage due to the Cr(VI) becomes limiting in the system. In a recent study by Du et al., 97.0% Cr(VI) removal percentage was observed, using 40 mg MnO_2 nanowires/diatomite from 100 mL of 20 mg L^{-1} (24).

Contact time is one of the most important parameters in the design of economical wastewater treatment systems. To studies the contact time, three different initial

concentrations of Cr(VI) ions were selected, 20, 70 and 140 mg L^{-1}. It can be seen from Figure 6, that adsorption efficiency of Cr(VI) ions increased rapidly with increase in contact time until the establishment of equilibrium between the metal ions adsorbed on the surface of $NiFe_2O_4$ nanoparticles and those present in the solution. After it reached the equilibrium, there were no important changes in metal ion concentrations. The adsorption took place more rapidly at initial phases and gradually slowed down as it reaches the equilibrium state. This behavior is quite usual because of the saturation of the available surface active sites. The experiments showed that the equilibrium was reached within 55 min for the Cr(VI) ions. Similar results were observed by Guo who studied the effect of contact time on removal of Cr(VI) from aqueous solution by amino functionalized magnetic graphenes composite material and indicated that adsorption increases with increasing contact time (9).

In order to discover the characteristics of the adsorption process in detail, the pseudo-first-order and pseudo-second-order kinetic models were used to determine the dynamics of the adsorption process. The pseudo-first-order and pseudo-second-order models can, respectively, be expressed by equations [3] and [4] (25):

$$\ln(q_e - q_t) = \ln(q_e) - \frac{k_1 t}{2.303} \quad (3)$$

$$\frac{t}{q_t} = \frac{1}{k_2 q_e^2} + \frac{t}{q_e} \quad (4)$$

whereq_e and q_t are the amount of Cr(VI) ions adsorbed (mg g^{-1}) at equilibrium and time t (min); k_1 is the rate constant of pseudo-first-order (min^{-1}); k_2 is the rate constant of pseudo-second-order (g mg^{-1} min^{-1}) for adsorption. The fitting curves and kinetic data were shown in Figure 7 and Table 1. According to the comparison of correlation coefficients (R^2) derived from two kind of models, the pseudo-second-order model was possessed of higher R^2 value at all the studied initial concentrations and thus could describe the best Cr(VI) ions adsorption on adsorbent. It is also seen that the fitting curves by pseudo-second-order equation matched better with the experimental data, further confirming the conclusion stated above. In addition, the experimental and theoretical values of q_e (obtained from pseudo-second-order model) are very close. All these results indicated the adsorption process in the study belonged to the pseudo-second-order kinetic model.

Adsorption isotherm portrayed how adsorbates interacted with adsorbents, which was critical in optimizing the practical use of adsorbents and realizing the adsorption process. To monitor the adsorption isotherm, Langmiur and Freundlich models were selected to research the equilibrium data. The linearized Langmiur isotherm equation (5) and Freundlich isotherm equation (6) can be expressed as follows (26, 27):

$$\frac{C_e}{q_e} = \frac{C_e}{q_m} + \frac{1}{q_m b_l} \quad (5)$$

$$\ln q_e = \frac{1}{n}\ln C_e + \ln k_f \quad (6)$$

where c_e (mg L^{-1}) is the equilibrium concentration of Cr(VI) ions in solution, q_e (mg g^{-1}) is the equilibrium adsorption capacity of $NiFe_2O_4$ nanoparticles, q_m (mg g^{-1}) is the maximum adsorption capacity of $NiFe_2O_4$ nanoparticles for monolayer coverage, b (L mg^{-1}) is a constant related to the adsorption free energy, K_f (mg^{l-}(1/n) L1/n g^{-1}) is a constant related to adsorption capacity and n is an empirical parameter which is related to adsorption. Values of isotherm model parameters are listed in Table 2.

The correlation coefficient (R^2) value was found greater than 0.99, which clearly showed the suitability of Langmuir model to describe the adsorption process (Figure 8a). This result showed the homogeneous nature of sample surface, i.e., each metal molecule adsorption has equal adsorption activation energy and it clearly demonstrated the formation of monolayer coverage of Cr(VI) ions on the outer

surface of $NiFe_2O_4$ nanoparticles. The maximum adsorption capacity (q_{max}) of Cr(VI) on the $NiFe_2O_4$ nanoparticles was calculated as 294.1 mg g^{-1} according to the Langmuir model. The Cr(VI) ions adsorption capacity was compared with other adsorbents in the literatures. High adsorption capacity of Cr(VI) was achieved by activated carbon 36 (28), $Al(OH)CO_3$ 60 (29), graphenes magnetic material 39.9 (9) and MnO_2 nanowires 152 (24), respectively. However, higher adsorption capacity was observed by the adsorbent ($NiFe_2O_4$ nanoparticles) prepared in this work.

For the Langmuir adsorption process, the influence of the isotherm shape on whether adsorption is favorable or unfavorable can be classified by a dimensionless separation factor R_L, which is considered as a more reliable indicator of the adsorption capacity. This constant is evaluated as:

$$R_L = \frac{1}{1+bC_0} \qquad (7)$$

Where C_0 is the maximal initial Cr(VI) concentration and b is the Langmuir adsorption constant (L mg^{-1}). The values of RL indicate the shapes of isotherms to be either unfavorable (R_L>1), linear (R_L=1), favorable (0 <R_L< 1) or irreversible (R_L=0). Favorable adsorption is reported when the R_L values are between 0 and 1. In the present work, the R_L value was 0.390 for Cr(VI) ions, which shows that the adsorption of Cr(VI) ions is favorable.

Conclusion

A new adsorbent was successfully prepared for Cr(VI) ions adsorption. SEM and BET analyses of the $NiFe_2O_4$ nanoparticles indicated that the surface morphology and surface area of $NiFe_2O_4$ nanoparticles can be useful for the adsorption of target adsorbate. The adsorption characteristics of the $NiFe_2O_4$ nanoparticles were well elucidated by batch adsorption of Cr(VI) ions from an aqueous solutions. These results demonstrate Cr(VI) ions adsorption onto $NiFe_2O_4$ nanoparticles via a monolayer adsorption on the homogeneous surface and was well described by rate-limiting pseudo-second-order kinetics. Also, the mechanism of adsorption can be explained by electrostatic attraction between the Cr(VI) ions and the $NiFe_2O_4$ nanoparticles.

Footnotes

Acknowledgments:

The author is grateful to the Hamedan Branch, Islamic Azad University for providing facilities to conduct and complete this study.

Conflict of Interest:

The authors stated no conflict of interest.

References

1. Shi M, Li Z, Yuan Y, Yue T, Wang J, Li R, et al. In situ oxidized magnetite membranes from 316L porous stainless steel via a two-stage sintering process for hexavalent chromium [Cr(VI)] removal from aqueous solutions.Chemical Engineering Journal. 2015;265:84-92.
2. Kaprara E, Seridou P, Tsiamili V, Mitrakas M, Vourlias G, Tsiaoussis I, et al. Cu-Zn powders as potential Cr (VI) adsorbents for drinking water. Journal of hazardous materials. 2013;262:606-13.
3. Kim MK, Sundaram KS, Iyengar GA, Lee K-P. A novel chitosan functional gel included with multiwall carbon nanotube and substituted polyaniline as adsorbent for efficient removal of chromium ion. Chemical Engineering Journal. 2015;267:51-64.
4. Hu J, Chen C, Zhu X, Wang X. Removal of chromium from aqueous solution by using oxidized multi walled carbon nanotubes. Journal of hazardous materials. 2009;162(2):1542-50.
5. Wu Y, Fan Y, Zhang M, Ming Z, Yang S, Arkin A, et al. Functionalized agricultural biomass as a low-cost adsorbent: Utilization of rice straw incorporated with amine groups for the adsorption of Cr (VI) and Ni (II) from single and binary systems. Biochemical Engineering Journal. 2016;105:27-35.
6. Lv G, Li Z, Jiang W-T, Ackley C, Fenske N, Demarco N. Removal of Cr (VI) from water using Fe (II)-modified natural zeolite. Chemical Engineering Research and Design. 2014;92(2):384-90.
7. Ng I-S, Wu X, Yang X, Xie Y, Lu Y, Chen C. Synergistic effect of Trichodermareeseicellulases on agricultural tea waste for adsorption of heavy metal Cr (VI). Bioresource technology. 2013;145:297-301.

8. Melita L, Popescu M. Removal of Cr (VI) from industrial water effluents and surface waters using activated composite membranes. Journal of Membrane Science. 2008;312(1):157-62.
9. Guo X, Du B, Wei Q, Yang J, Hu L, Yan L, et al. Synthesis of amino functionalized magnetic graphenes composite material and its application to remove Cr (VI), Pb (II), Hg (II), Cd (II) and Ni (II) from contaminated water. Journal of hazardous materials. 2014;278:211-20.
10. Sobhanardakani S, Parvizimosaed H, Olyaie E. Heavy metals removal from wastewaters using organic solid waste—rice husk. Environmental Science and Pollution Research. 2013;20(8):5265-71.
11. Sobhanardakani S, Zandipak R, Fili Z, Ghoochian M, Sahraei R, Farmany A. Removal of V (V) ions from aqueous solutions using oxidized multi-walled carbon nanotubes. 2015.
12. Zhang Z, Zhang H, Zhu L, Zhang Q, Zhu W. Hierarchical porous $Ca(BO_2)_2$ microspheres: Hydrothermal–thermal conversion synthesis and their applications in heavy metal ions adsorption and solvent-free oxidation of benzyl alcohol. Chemical Engineering Journal. 2016;283:1273-84.
13. Sobhanardakani S, Zandipak R. 2, 4-Dinitrophenylhydrazine functionalized sodium dodecyl sulfate-coated magnetite nanoparticles for effective removal of Cd (II) and Ni (II) ions from water samples. Environmental monitoring and assessment. 2015;187(7):1-14.
14. Madrakian T, Afkhami A, Zadpour B, Ahmadi M. New synthetic mercaptoethylaminohomopolymer-modified maghemite nanoparticles for effective removal of some heavy metal ions from aqueous solution.Journal of Industrial and Engineering Chemistry. 2015;21:1160-6.
15. Ding Y, Zhu L, Wang N, Tang H. Sulfate radicals induced degradation of tetrabromobisphenol A with nanoscaled magnetic $CuFe_2O_4$ as a heterogeneous catalyst of peroxymonosulfate. Applied Catalysis B: Environmental. 2013;129:153-62.
16. Pan W, Gu F, Qi K, Liu Q, Wang J. Effect of Zn substitution on morphology and magnetic properties of $CuFe_2O_4$ nanofibers. Materials Chemistry and Physics. 2012;134(2):1097-101.
17. Huang Z, Yin G, Liao X, Yao Y, Kang Y. Preparation and magnetic properties of Cu-ferrite nanorods and nanowires. Journal of Colloid and Interface Science. 2008;317(2):530-5.
18. Zandipak R, Sobhanardakani S. Synthesis of NiFe2O4 nanoparticles for removal of anionic dyes from aqueous solution. Desalination and Water Treatment. 2015(ahead-of-print):1-13.
19. Sobhanardakani S, Zandi Pak R, Mohammadi MJ. Removal of Ni(II) and Zn(II) from Aqueous Solutions Using Chitosan. Archives of Hygiene Sciences. 2016;5(1):47-55.
20. Asadi F, Dargahi A, Almasi A, Moghofe E. Red Reactive 2 Dye Removal from Aqueous Solutions by Pumice as a Low-Cost and Available Adsorbent. Archives of Hygiene Sciences. 2016;5(3):145-52.
21. Brunauer S, Emmett PH, Teller E. Adsorption of gases in multimolecular layers. Journal of the American chemical society. 1938;60(2):309-19.
22. Venkatesha T, Viswanatha R, Nayaka YA, Chethana B. Kinetics and thermodynamics of reactive and vat dyes adsorption on MgO nanoparticles. Chemical Engineering Journal. 2012;198:1-10.
23. Liu Y-q, Liu Y-g, Hu X-j, Guo Y-m. Adsorption of Cr(VI) by modified chitosan from heavy-metal polluted water of Xiangjiang River, China. Transactions of Nonferrous Metals Society of China. 2013;23(10):3095-103.
24. Du Y, Zheng G, Wang J, Wang L, Wu J, Dai H. MnO 2 nanowires in situ grown on diatomite: Highly efficient absorbents for the removal of Cr (VI) and As (V). Microporous and Mesoporous Materials. 2014;200:27-34.
25. Azizian S. Kinetic models of sorption: a theoretical analysis. Journal of colloid and Interface Science. 2004;276(1):47-52.
26. Langmuir I. The adsorption of gases on plane surfaces of glass, mica and platinum.Journal of the American Chemical society. 1918;40(9):1361-403.
27. Freundlich H, Heller W. The adsorption of cis-and trans-azobenzene.Journal of the American Chemical Society. 1939;61(8):2228-30.
28. Cao C-Y, Cui Z-M, Chen C-Q, Song W-G, Cai W. Ceria hollow nanospheres produced by a template-free microwave-assisted hydrothermal method for heavy metal ion removal and catalysis. The Journal of Physical Chemistry C. 2010;114(21):9865-70.
29. Zhong L-S, Hu J-S, Cao A-M, Liu Q, Song W-G, Wan L-J.3D flowerlike ceria micro/nanocomposite structure and its application for water treatment and CO removal.Chemistry of Materials. 2007;19(7):1648-55.